GEOPHYSICAL RESEARCH LETTERS, VOL. 34, L16315, doi:10.1029/2007GL030548, 2007

Click Here for Full Article

Inferring fault characteristics using fold geometry constrained by Airborne Laser Swath Mapping at Raplee Ridge, Utah

I. Mynatt,[1] G. E. Hilley,[1] and D. D. Pollard[1]

Received 7 May 2007; revised 29 June 2007; accepted 10 July 2007; published 29 August 2007.

[1] We used Airborne Laser Swath Mapping (ALSM) data to define the geometry of strata in Raplee Ridge in southeastern Utah that were likely deformed by slip on an underlying fault. The fold geometry was used to infer the fault geometry and loading responsible for the folding using the Boundary Element Model, Poly3D. Monte Carlo Markov-Chain (MCMC) methods created probability density functions (pdfs) that reveal the most likely fault geometry and loading conditions and their uncertainties. Despite the restrictive assumptions of Poly3D, in which body deformations occur from slip on displacement discontinuities in a homogeneous linear-elastic half-space, the strata deflections are matched remarkably well, and the resulting inferences of fault geometry and stress field appear reasonable. We propose that similar methods may be used with models that include more complicated rheologies and heterogeneous and anisotropic material properties to estimate fault geometries and loading conditions where only deflection of strata record these parameters. **Citation:** Mynatt, I., G. E. Hilley, and D. D. Pollard (2007), Inferring fault characteristics using fold geometry constrained by Airborne Laser Swath Mapping at Raplee Ridge, Utah, *Geophys. Res. Lett.*, *34*, L16315, doi:10.1029/2007GL030548.

1. Introduction

[2] Slip along blind thrust faults deforms the surrounding rock mass, often resulting in large deflections of the overlying sedimentary layers [*Bullard and Lettis*, 1993; *King et al.*, 1988; *Roering et al.*, 1997; *Stein and Yeats*, 1989]. The style and geometry of this deformation depends on the fault geometry, the slip distribution and magnitude, and the rheology of the rock in which it is embedded. Structural geologists have used forward numerical models to investigate how stress and deformation fields change with variations in these factors [e.g., *Cooke and Pollard*, 1997; *Segall and Pollard*, 1980; *Willemse et al.*, 1996], while geodesists typically use inverse methods to estimate the geometry of and slip rates along faults from observed surface displacement rates [*Bürgmann et al.*, 2005; *Harris and Segall*, 1987; *Maerten et al.*, 2005]. Deformation observed in exhumed field analogues and in seismic reflection data as well as earthquake seismicity can supply modeling constraints to estimate the geometry of faults that may produce the observed deformations [*Ekström et al.*, 1992; *Namson and Davis*, 1994; *Stein*, 1995], and indeed, kinematic models have been employed for such purposes [*Allmendinger*, 1998; *Narr and Suppe*, 1994]. However, by their nature, kinematic models cannot be used to estimate the loading conditions that resulted in slip along a fault, may yield non-unique combinations of fault geometries and slip, and may produce untenable particle paths [*Johnson and Johnson*, 2002]. Thus, the development of an inversion method that uses the fold geometry with consideration of momentum conservation, rheological properties and material continuity to estimate fault geometry and loading conditions appears timely.

[3] In this contribution, we develop such a method and present an example of its application to the Raplee Ridge fold in southeastern Utah. Like many fold structures of the Colorado Plateau, the partially-exhumed fold likely formed by slip on a blind reverse fault induced by Laramide contraction [*Gregory and Moore*, 1931]. We use Airborne Laser Swath Mapping (ALSM) data provided by the National Center for Airborne Laser Mapping (NCALM) to map the deflection of sedimentary layers overlying the proposed fault and use this deflection to estimate the fault geometry and stress conditions that created the fold. Also, we estimate the uncertainties in these parameters and how they vary with one another. We suggest that similar approaches may be used to infer the geometry and loading of other blind thrust faults where surface and/or subsurface data only resolve distributed deformation (such as folding) in the rock mass, rather than the geometry of an underlying fault.

2. Raplee Ridge Field Site

[4] The deformation at Raplee Ridge, located in the Four Corners area of the southwestern USA (Figure 1a) resulted in the deflection of Pennsylvanian and Permian limestones, sandstones and shales (Figure 2a). The 500-m-high fold is roughly monoclinal in cross section with an amplitude of ~500 m, and is characterized by a steeply west dipping (up to 40°) forelimb and a shallow (<5°) backlimb. The flexure terminates as plunging noses at both ends of its ~14 km length. The shape of the fold is well defined by the McKim Limestone, the uppermost unit of the ~140 m thick Rico Formation. This 1–3 m thick layer is underlain by a thin (~8 m) shale unit of the Rico Formation and is overlain by the massive (~120 m) Halgaito Tongue Shale. The fissility of the Halgaito Tongue Shale has resulted in its erosion from much of the fold exposing the more resistant underlying McKim. The upper bedding surface of the McKim, therefore, is exposed across both limbs, along sections of the hinge, and extensively in both the southern and northern noses. Although exposure of the McKim Limestone is extensive in some areas, in others, such as the fold hinge and in the steeper portions of the forelimb, the top of the

[1]Department of Geological and Environmental Sciences, Stanford University, Stanford, California, USA.

Copyright 2007 by the American Geophysical Union.
0094-8276/07/2007GL030548$05.00

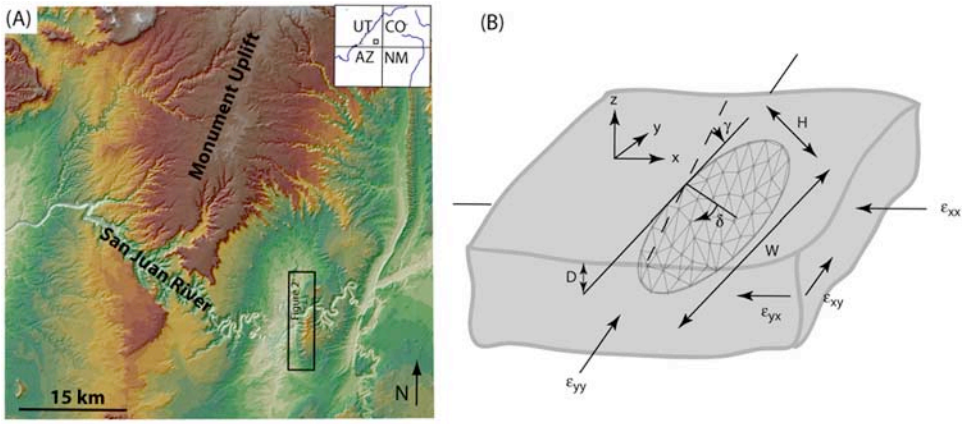

Figure 1. (a) Location of Raplee Ridge in southeastern Utah. Location and extent of the ALSM dataset is denoted by the labeled box. (b) Definition of variables used to define model fault geometry and remote strain conditions.

unit is only expressed as small ledges projecting decimeters from cliff faces or steep slopes.

3. Methods

[5] NCALM acquired ALSM data over Raplee Ridge on February 24, 2005. The lack of vegetation at the field site rendered bare-earth filtering unnecessary. Individual points have accuracies of <10 cm for the altitude at which these data were acquired. These dense point measurements (typically >3 points per m^2) were interpolated to form a 1-m grid of elevations over the area. The overall fold shape is evident in the topography and individual units within the Rico Formation are expressed both as large pavements (unit tops) and small breaks in slope (unit edges) (Figures 2a and 2b). ALSM data were used for this study because of the ability to identify particular lithologic units that would be difficult or impossible to locate in less precise data sets, such as 10 or 30 m DEM's.

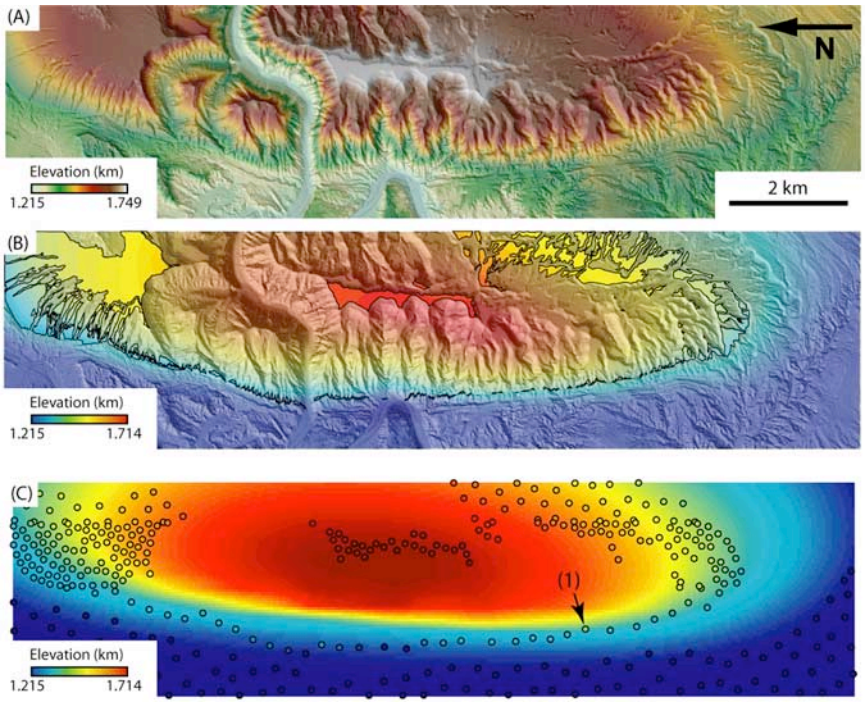

Figure 2. (a) ALSM data collected by NCALM, shaded for relief. (b) Mapped remnants of the McKim surface (vibrant areas) and interpolated surface (using a minimum curvature spline to points; faded areas) overlain on shaded relief map of Raplee Ridge. (c) Best-fit deflected surface (assuming an initially flat stratigraphy) compared with points extracted from the McKim surface (circles) that were used to estimate the underlying fault geometry and remote loading conditions. Each of the selected points is color-coded for measured elevation and so the difference in color between these measured points and the surrounding modeled deflections provides a gauge of model misfit. For example, the deflection at the point labeled (1) is not matched well by the best-fitting model, and so its color deviates significantly from the background coloring.

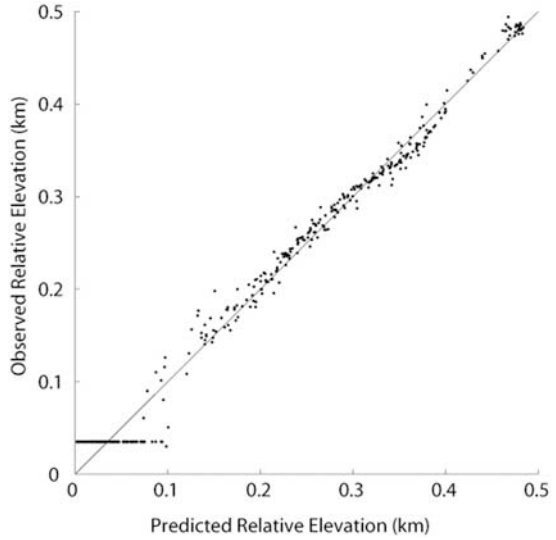

Figure 3. Observed versus predicted (modeled) elevations for points highlighted in Figure 2a. The lowest line of poorly fitting points is an artifact of the extrapolation of the McKim surface into the subsurface. Because the McKim surface was unexposed in the forelimb of the fold, we used the geometry of higher stratigraphic surfaces with the measured stratigraphic thickness to infer the depth of the McKim below the surface. These depths were used as inputs to the model evaluations, and the relative uniformity of their values results from the simple extrapolations of this surface.

[6] We mapped the McKim by creating a large hill-shaded printout of the ALSM data and mapped the unit onto this shaded relief base in the field. Erosion and deposition sometimes made the top of the McKim difficult to identify. For this reason the vertical accuracy of the field mapping for the one to three meter thick McKim limestone [*Ziony*, 1966] was estimated as 1 m. The McKim limestone is a grey calcisiltite and is part of the Rico Formation, a regressionary sequence. The sediments of the Rico are thought to be near shore shelf deposits and therefore initially approximately flat lying [*Ziony*, 1966]. This assumption is supported by the undeformed outcrops of the Rico near Raplee Ridge which exhibit near horizontal dips.

[7] Points (shown in Figure 2c) from the top of the McKim were used to reconstruct the deflection of this surface. Deflections expected due to various fault geometries and loading conditions were modeled using the Boundary Element Method (BEM) code called Poly3D [*Thomas*, 1993], which calculates the expected strains, stresses, and displacements in a linear-elastic half-space surrounding a fault under either imposed remote stresses or strains, or specified slip. We calculated deflections for different directions and magnitudes of the remote principle stresses, and for different fault geometries. These model deflections were compared to those inferred from our mapping and ALSM analysis using the following cost function:

$$P\left(x|H,W,D,x_o,,y_o,\gamma,\delta,\varepsilon_{xx},\varepsilon_{xy},\varepsilon_{yy},o\right)=\exp\left(\sum_{i=1}^{n}\frac{-(o_i-x_i)^2}{\sigma_i^2}\right) \quad (1)$$

where ε_{xx}, ε_{xy}, ε_{yy} are the components of the remote strain tensor (contraction negative, ε_{zz}, ε_{xz}, and ε_{yz} assumed zero), H is the fault down-dip length, W is the width along strike, D is the depth of the upper tip of the fault below the surface, γ is the strike of the fault, δ is its dip, o are the observed (field) deflections (at circles in Figure 2c), x are the predicted (modeled) deflections, σ is the variance associated with each measurement (see below), and n is the number of points for which deflection has been measured (Figure 1b). We used a Poisson's ratio of 0.25; the magnitudes of the remote stresses scale with, and so were normalized to the shear modulus.

[8] Equation 1 provides the means of calculating the probability of observing the modeled deflections given the parameters representing the fault geometry and loading. Maximizing $P(x|H, W, D, x_o, y_o, \gamma, \delta, \varepsilon_{xx}, \varepsilon_{xy}, \varepsilon_{yy}, o)$ by changing the fault geometry and loading parameters identifies the best-fit model, and Bayesian methods may be used to quantify uniqueness, uncertainty, and covariation between these factors [e.g., *Hilley et al.*, 2005; *Johnson and Segall*, 2004]. In this study we find both the best fitting model geometry and loading, but also use a Metropolis-Hastings Markov-Chain Monte Carlo sampling method [e.g., *Lewis*, 2001; *Metropolis et al.*, 1953] to determine the probability densities of the parameters that encapsulate this geometry and loading. This sampling procedure chooses future parameter combinations based on the misfit calculated for a given simulation, and in so doing, the density of all simulated parameter combinations approximates the probability density of these parameters that is permissible by the observations. Thus, we can evaluate not only the best-fitting combination of geometric and loading parameters, but also how these parameters covary and how well defined they might be.

4. Results

[9] The deflection resulting from the best-fitting combination of fault geometry and loading conditions that reproduced the observed folding at Raplee Ridge is shown in Figure 2c. Because we chose an isotropic, linear-elastic rheology, the magnitudes of the remote (tectonic) strains must increase as model fault slip and marker horizon deflection increases. In nature, the fault can only accommodate a small strain change in each of many discrete slip episodes, between which the tectonic strain continues to accumulate. The magnitudes of the local model stresses calculated for the ~500 meters of deflection observed at Raplee Ridge are unreasonably large (on the order of several GPa) relative to those that likely develop in one slip episode along the fault (typically on the order of 10's of MPa; e.g., *Zoback et al.* [1987]). In nature, these stress perturbations relax during the interseismic period due to viscoelastic deformation or brittle fracture [e.g., *Johnson and Segall*, 2004; *Savage and Prescott*, 1978].

[10] In general, the overall shape and magnitude of the fold was well captured by the approach used here (Root Mean Square Error (RMSE) of 16.3 m) (Figure 3). Specifically, the parameters for the best-fit model are reasonable given the geologic and tectonic history of this fold. The model fault strikes 3.3° and dips 44.1° to the east. The upper fault tip is 0.8 km below the initially flat-lying McKim

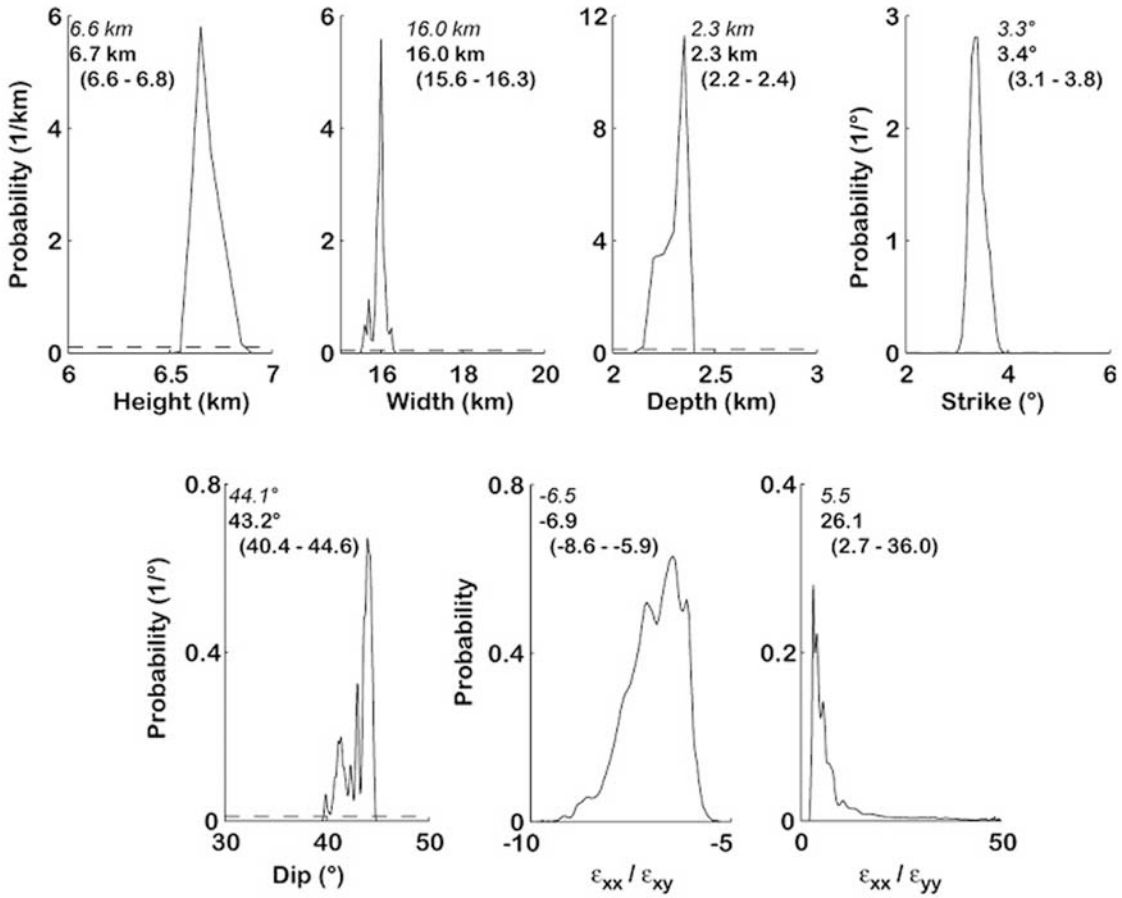

Figure 4. Probability density functions (pdfs) of fault geometry and remote loading parameters that were found using the MCMC simulations. The best-fit combination of these parameters are shown in each panel in italics, the mean values of the MCMC simulations are shown in bold, and the upper and lower 95% ranges in the inferred model parameters are shown in parentheses. The McKim limestone was likely ~1.5 km below the surface prior to deformation and so the depth of the fault below the McKim must be adjusted by this amount.

surface, and it is 6.6 km wide and 16 km in down-dip length. The magnitude of ε_{xx} is ~6 times greater than ε_{yy} or ε_{xy}.

[11] Importantly, the RMSE for the best-fitting model produces average misfits that are over an order-of-magnitude greater than the precision of the ALSM data. In other words, the data are considerably more precise than the model. Should we choose to use the inherent precision of the ALSM data to estimate the variance in the model parameters (equation 1), these estimates would be far more conservative than the simple linear elastic model warrants.

[12] To include the uncertainties inherent in the model, we used the RMSE as a measure of variance in the data (σ in equation 1). We sampled the model parameter space 100,000 times after an initial burn-in period of 10,000 simulations, [e.g., *Buck et al.*, 1996] to provide an estimate of the uncertainties in the model parameters (Figure 4). The mean model parameter values calculated using equation 1 closely resemble those of the best-fitting set of parameters, and the variance in most parameters was surprisingly small (Figure 4). The one exception to this was the ratio of ε_{xx} to ε_{yy}, in which the best-fitting value for this parameter was a factor of ~5 less than its mean value. This arises from the fact that ε_{yy} is poorly constrained by our analysis, as might be expected. The strike of the monocline approximately coincides with the y-coordinate direction and this results in poor definition of the resolved tractions along the fault.

5. Discussion and Conclusions

[13] Methods that have used geologic data to infer past regional strain orientations are not new, but the simultaneous inversions of geologic data for fault geometry and the relative magnitudes of the tectonic strain tensor are. In addition, the method introduced here provides a means of inferring tectonic loading conditions that caused slip on faults of a variety of scales, rather than using the orientation and slip directions along small faults to estimate regional loading [e.g., *Reches et al.*, 1992]. These latter methods may be sensitive to local perturbations in the stress field that result from the presence of surrounding, active geologic structures and heterogeneities in mechanical properties [e.g., *Pollard et al.*, 1993]. While the same may also be said of the methods developed here, the larger scale of structures such as the Raplee Ridge fold are more likely to reflect regional loading.

[14] While the method provides a new way of imaging the geometry of subsurface faults and the tectonic loading that induced slip, we acknowledge several potential limitations that are embedded in the Poly3D linear-elastic

dislocation model. In particular, Poly3D idealizes the upper crust as a homogeneous linear elastic material whose field quantities are continuous at all points except at those along the faults. The faults experience unrealistically great stress drops to produce the slip observed. Secondly, folds in sedimentary strata are likely anisotropic in their mechanical behavior due to the role of bedding plane slip and the enhanced compliance of soft, fine-grained sedimentary strata. Third, faults are not frictionless so the model fault slips more under a given tectonic strain than a natural fault would. Thus, we underestimate the tectonic strain necessary to product the fold. Finally, the linear-elastic rheology does not allow strain localization by mechanisms such as strain weakening of the material—this may prevent the localization of deformation in the fold's hinge, causing the inferred location of the model fault to be farther from the deflected layer than it actually may be.

[15] Nonetheless, the deflections predicted by the best-fit model produce a remarkable match to those observed in the field (Figure 3). An interesting extension of this work would be to use the inverse methods developed in this study with a set of different mechanical models that consider a range of rheologies. Using this approach, we might be able to invert for appropriate rheological properties.

References

Allmendinger, R. W. (1998), Inverse and forward numerical modeling of trishear fault-propagation folds, *Tectonics*, *17*, 640–656.

Buck, C. E., et al. (1996), *The Bayesian Approach to Interpreting Archeological Data*, 382 pp., Wiley, Chichester, U. K.

Bullard, T. F., and W. R. Lettis (1993), Quaternary fold deformation associated with blind thrust faulting, Los Angeles Basin, California, *J. Geophys. Res.*, *98*, 8349–8369.

Bürgmann, R., M. G. Kogan, G. M. Steblov, G. Hilley, V. E. Levin, and E. Apel (2005), Interseismic coupling and asperity distribution along the Kamchatka subduction zone, *J. Geophys. Res.*, *110*, B07405, doi:10.1029/2005JB003648.

Cooke, M. L., and D. D. Pollard (1997), Bedding-plane slip in initial stages of fault-related folding, *J. Struct. Geol.*, *19*, 567–581.

Ekström, G., R. S. Stein, J. P. Eaton, and D. Eberhart-Phillips (1992), Seismicity and geometry of a 110-km-long blind thrust fault: 1. The 1985 Kettleman Hills, California, earthquake, *J. Geophys. Res.*, *97*, 4843–4864.

Gregory, H. E. and R. C. Moore (1931), The Kaiparowits Regions, a geographic and geologic reconnaissance of parts of Utah and Arizona, *U.S. Geol. Surv. Prof. Pap.*, *164*.

Harris, R., and P. Segall (1987), Detection of a locked zone at depth on the Parkfield, California, segment of the San Andreas fault, *J. Geophys. Res.*, *92*, 7945–7962.

Hilley, G. E., R. Bürgmann, P.-Z. Zhang, and P. Molnar (2005), Bayesian inference of plastosphere viscosities near the Kunlun Fault, northern Tibet, *Geophys. Res. Lett.*, *32*, L01302, doi:10.1029/2004GL021658.

Johnson, K. M., and A. M. Johnson (2002), Mechanical models of trishear-like folds, *J. Struct. Geol.*, *24*, 277–287.

Johnson, K. M., and P. Segall (2004), Viscoelastic earthquake cycle models with deep stress-driven creep along the San Andreas fault system, *J. Geophys. Res.*, *109*, B10403, doi:10.1029/2004JB003096.

King, G., R. S. Stein, and J. B. Rundle (1988), The growth of geological structures by repeated earthquakes: 1. Conceptual framework, *J. Geophys. Res.*, *93*, 13,307–13,318.

Lewis, P. O. (2001), Phylogenetic systematics turns over a new leaf, *Trends Ecol. Evol.*, *16*, 30–37.

Maerten, F., et al. (2005), Inverting for slip on three-dimensional fault surfaces using angular dislocations, *Bull. Seismol. Soc. Am.*, *95*, 1654–1665.

Metropolis, N., et al. (1953), Equations of state calculations by fast computing machines, *J. Chem. Phys.*, *21*, 1087–1091.

Namson, J., and T. L. Davis (1994), A balanced cross-section of the 1994 Northridge earthquake, southern California, *Nature*, *372*, 167–169.

Narr, W., and J. Suppe (1994), Kinematics of basement-involved compressive structures, *Am. J. Science*, *294*, 802–860.

Pollard, D. D., et al. (1993), Stress inversion methods: Are they based on faulty assumptions?, *J. Struct. Geol.*, *15*, 1045–1054.

Reches, Z., G. Baer, and Y. Hatzor (1992), Constraints on the strength of the upper crust from stress inversion of fault slip data, *J. Geophys. Res.*, *97*, 12,481–12,493.

Roering, J. J., M. L. Cooke, and D. D. Pollard (1997), Why blind thrust faults do not propagate to the Earth's surface: Numerical modeling of coseismic deformation associated with thrust-related anticlines, *J. Geophys. Res.*, *102*, 11,901–911,912.

Savage, J. C., and W. H. Prescott (1978), Asthenosphere readjustment and the earthquake cycle, *J. Geophys. Res.*, *83*, 3369–3376.

Segall, P., and D. D. Pollard (1980), Mechanics of discontinuous faults, *J. Geophys. Res.*, *85*, 4337–4350.

Stein, R. S. (1995), Northridge earthquake: Which fault and what next?, *Nature*, *373*, 388–389.

Stein, R. S., and R. S. Yeats (1989), Hidden earthquakes, *Sci. Am.*, *260*, 48–57.

Thomas, A. L. (1993), Poly3D: A three-dimensional, polygonal element, displacement discontinuity boundary element computer program with applications to fractures, faults, and cavities in the Earth's crust, master's thesis, 221 pp., Stanford Univ., Stanford, Calif.

Willemse, E. J. M., et al. (1996), Three-dimensional analyses of slip distributions on normal fault arrays with consequences for fault scaling, *J. Struct. Geol.*, *18*, 295–309.

Ziony, J. I. (1966), Analysis of systematic jointing in part of the Monument Upwarp, southeastern Utah, Ph.D. thesis, 152 pp, Univ. of Calif., Los Angeles.

Zoback, M. D., et al. (1987), New evidence on the state of stress of the San Andreas fault system, *Science*, *238*, 1105–1111.

G. E. Hilley, I. Mynatt, and D. D. Pollard, Department of Geological and Environmental Sciences, Stanford University, 450 Serra Mall Building 320, Stanford, CA 94305-2115, USA. (imynatt@pangea.stanford.edu)